Capillary jet breakup by noise amplification

S. Le Dizès[1,†] and E. Villermaux[1,2]

[1]Aix Marseille Univ, CNRS, Centrale Marseille, IRPHE, Marseille, France
[2]Institut Universitaire de France, Paris, France

A liquid jet falling by gravity ultimately destabilizes by capillary forces. Accelerating as it falls, the jet thins and stretches, causing a capillary instability to develop on a spatially varying substrate. We discuss quantitatively the interplay between instability growth, jet thinning and longitudinal stretching for two kinds of perturbations, either solely introduced at the jet nozzle exit or affecting the jet all along its length. The analysis is conducted for any values of the liquid properties for a sufficiently large flow rate. In all cases, we determine the net gain of the most dangerous perturbation for all downstream distances, thus predicting the jet length, the wavelength at breakup and the resulting droplet size.

Key words: capillary flows, interfacial flows (free surface)

---

1. Introduction

Seemingly simple questions are not always the simplest to answer quantitatively. A canonical illustration of this affirmation is the apparently simple problem of a liquid thread, falling from a nozzle by its own weight under the action of gravity, as shown in figure 1. As it falls, the thread eventually fragments into drops, a fact that we understand because locally it has a columnar shape, and thus suffers a capillary instability. However, how far from the nozzle exit does breakup happen? Even a distracted look at the possible scenarios lets one glimpse the potential difficulties of a precise analysis: a distance z is the product of a velocity u by a time τ,

$$z = u\tau. \tag{1.1}$$

Capillary breakup occurs within a time τ which depends on the thread radius h, the liquid density ρ, the viscosity η and the surface tension γ, and we know that most of this time is spent in developing an instability about the quasicolumnar shape of the thread, the subsequent phenomena occurring around the pinching instant at the drop separation being comparatively much faster (Eggers & Villermaux 2008). The time τ is either the capillary time $\sqrt{\rho h^3/\gamma}$ when inertia and surface tension are solely at play, or the viscous capillary time $\eta h/\gamma$ if viscous effects dominantly slow down the unstable dynamics. When the jet issues from the nozzle ballistically, keeping its velocity and radius constant, the problem is indeed simple, and amounts

† Email address for correspondence: ledizes@irphe.univ-mrs.fr
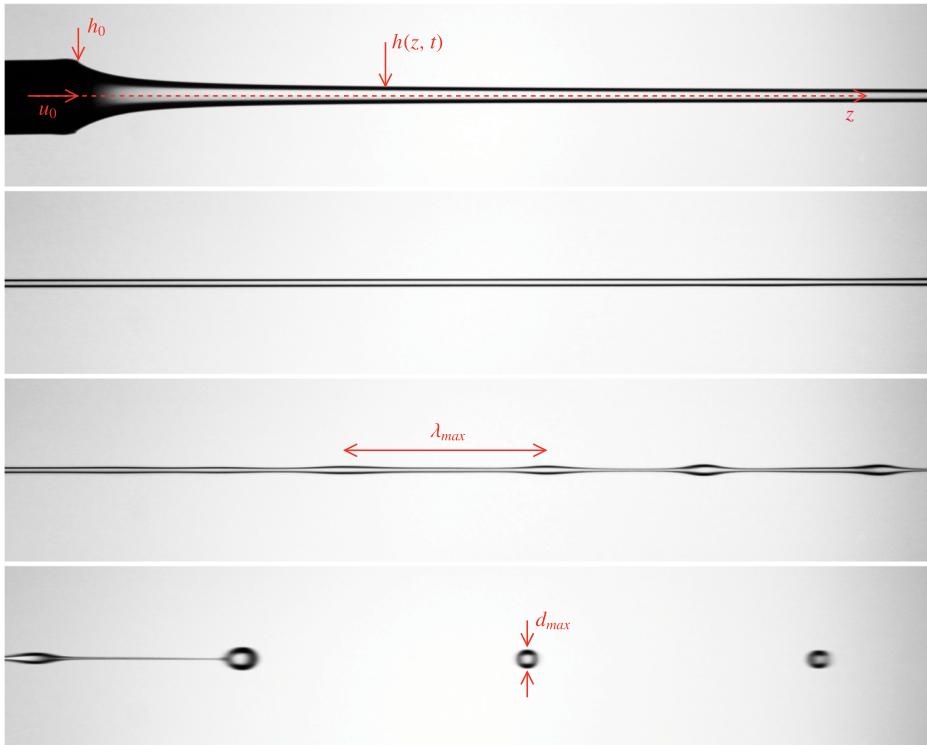
FIGURE 1. (Colour online) Four successive panels showing a liquid jet (density 950 kg m^{-3}, viscosity $\eta = 50 \times 10^{-3}$ Pa s) issuing from a round tube with radius $h_0 = 2$ mm at velocity $u_0 = 1$ cm s^{-1}, stretching in the gravity field (aligned with the z direction), and thinning as it destabilizes through the growth of bulges separated by λ_{max} at breakup, producing stable drops of diameter d_{max}.

to correct estimation of the relevant time scale τ to compute the so-called 'liquid intact length' of the jet (see the corresponding section in Eggers & Villermaux (2008) for a complete discussion and experimental references, including the case when the jet suffers a shear instability with the surrounding environment). Subtleties arise when the axial velocity of the jet depends on the axial distance z.

  A jet falling in the direction of gravity accelerates. If fed at a constant flow rate at the nozzle, stationarity implies that the thread radius thins with increasing distance from the exit. Therefore, if both u and h depend on the downstream distance, which estimates will correctly represent the breakup distance z in (1.1): those at the nozzle exit, those at the breakup distance or a mixture of the two? As the radius thins, the instability may switch from an inertia dominated régime to a viscous dominated régime. Then, which time scale τ should be considered to compute z?

  The detailed problem is even more subtle: the capillary instability preferentially amplifies a varicose perturbation, adjacent bulges along the thread feeding on the thinner ligament linking them (figure 1). The most amplified wavelength is proportional to h, the other wavelengths having a weaker growth rate. Since the jet accelerates, mass conservation of the incompressible liquid also implies that the distance between two adjacent instability crests increases with larger distances from the nozzle exit. The capillary instability has thus to compete with another

phenomenon, namely jet stretching, characterized by another time scale $(\partial_z u)^{-1}$. There are thus three time scales that may potentially contribute to τ, which all depend intrinsically on the distance from the nozzle. Deciding *a priori* which one will dominate and how is a hazardous exercise.

Deciphering of the relative importance of the coupled effects mentioned above requires an instability analysis accounting for both the substrate deformation (jet stretching) and the modification of the local instability dispersion relation as the jet thins (to describe the growing relative influence of viscosity). This question has been envisaged in the very viscous limit by Tomotika (1936), for the particular case where u increases linearly with z by Frankel & Weihs (1985, 1987) and more recently by Sauter & Buggisch (2005), Senchenko & Bohr (2005) and Javadi *et al.* (2013) for a gravitationally accelerated jet.

These last authors quantified the maximum gain that perturbations can reach at a given location using a local plane wave decomposition (WKBJ approximation). By choosing adequately the gain needed for breakup, they were able to collapse measurements of the breakup distance on a theoretical curve. They also obtained an asymptotic expression in the viscous régime consistent with the anticipated scaling law, which compares the viscous capillary time scale based on the current jet radius with the stretching time of the jet.

In the present work, we use a similar approach to that of Javadi *et al.* (2013) by searching for maximum perturbation gains using WKBJ approximations. In addition to providing much more detail, we extend their analysis in several ways. We first consider all of the régimes ranging from very viscous to inviscid. We then compare the maximum gain and the most dangerous frequency of the perturbations for two types of excitation: (1) nozzle excitation (the perturbation is introduced at the nozzle only) and (2) background noise (the perturbation is present everywhere). We finally provide predictions for the breakup wavelength and the resulting droplet size.

The paper is organized as follows. In §2, we present the mathematical formulation by providing the model for the base flow and the perturbations. An expression of the perturbation gain is derived using the WKBJ framework. In §3, the result of the optimization procedure maximizing the gain is provided for each type of excitation. The breakup distance, the most dangerous frequency, the wavelength and the droplet size are analysed as functions of the gain and fluid viscosity (Ohnesorge number *Oh*). Asymptotic formulae for weak and strong viscosity (small and large *Oh*) are provided in this section, though their derivation is given in an appendix at the end of the paper. For nozzle excitation, a peculiar behaviour of the optimal perturbation observed for intermediate Ohnesorge numbers ($0.1 < Oh < 1$) is further discussed in §4. We show that the peak of the breakup wavelength obtained for $Oh \approx 0.3$ is related to a property of the local dispersion relation outside the instability band. The results are compared with local predictions in §5 and applied to realistic configurations in §6.

2. Mathematical formulation

We consider an axisymmetric liquid jet falling vertically by the action of gravity g. The jet has a radius h_0 and a characteristic velocity u_0 at the nozzle (figure 1). The fluid has a density ρ, a viscosity $\nu = \eta/\rho$ and a surface tension γ. The surrounding environment is considered as evanescent, and is neglected.

2.1. *Base flow*

Spatial and time variables are non-dimensionalized using the radius h_0 and the capillary time $\tau_c = \sqrt{\rho h_0^3 / \gamma}$ respectively. The base flow is governed by three

parameters:

$$Q = u_0 \sqrt{\frac{\rho h_0}{\gamma}}, \quad \text{the flow rate,} \tag{2.1a}$$

$$Oh = \nu \sqrt{\frac{\rho}{\gamma h_0}}, \quad \text{the Ohnesorge number,} \tag{2.1b}$$

$$Bo = \frac{\rho g h_0^2}{\gamma} \quad \text{the Bond number.} \tag{2.1c}$$

One could alternatively use the Weber number $We = Q^2$ instead of the dimensionless flow rate. The Ohnesorge number is the ratio of the viscous capillary time scale to the capillary time scale. We describe the liquid jet by the one-dimensional model (Trouton 1906; Weber 1931; Eggers & Villermaux 2008)

$$\frac{\partial A}{\partial t} + \frac{\partial (Au)}{\partial z} = 0, \tag{2.2a}$$

$$\frac{\partial u}{\partial t} + u \frac{\partial u}{\partial z} = 3Oh \frac{1}{A} \frac{\partial}{\partial z} \left(A \frac{\partial u}{\partial z} \right) + \frac{\partial K}{\partial z} + Bo, \tag{2.2b}$$

with

$$K = \frac{4AA_{zz} - 2A_z^2}{[4A + A_z^2]^{3/2}} - \frac{2}{[4A + A_z^2]^{1/2}}, \tag{2.3}$$

where $u(z, t)$ is the local axial velocity, $A = h^2$ is the square of the local radius $h(z, t)$, z is the axial coordinate oriented downward, t is the time variable, and A_z and A_{zz} are respectively the first and second derivatives of A with respect to z. The boundary conditions at the nozzle are

$$A(z = 0, t) = 1, \quad u(z = 0, t) = Q. \tag{2.4a,b}$$

The stationary base flow satisfies

$$\frac{\partial (A_0 U_0)}{\partial z} = 0, \tag{2.5a}$$

$$U_0 \frac{\partial U_0}{\partial z} = 3Oh \frac{1}{A_0} \frac{\partial}{\partial z} \left(A_0 \frac{\partial U_0}{\partial z} \right) + \frac{\partial K_0}{\partial z} + Bo. \tag{2.5b}$$

The first equation gives

$$A_0 U_0 = Q. \tag{2.6}$$

We will consider the régime where the jet base flow is inertial and is given at leading order by

$$U_0 \frac{\partial U_0}{\partial z} = Bo. \tag{2.7}$$

This hypothesis amounts to neglecting viscous and curvature effects in the jet evolution. Because it accelerates as it falls, the jet gets thinner and slenderer. Curvature effects along z thus soon vanish (unless the jet is initially very small, see Rubio-Rubio, Sevilla & Gordillo 2013), and viscous stresses applying on the jet cross-section are also soon overcome by the gravity force (beyond a physical distance

from the nozzle of order $\sqrt{\nu u_0/g}$, see Clarke 1969). Equations (2.6) and (2.7) thus give

$$U_0(z) = \sqrt{2Boz + Q^2}, \tag{2.8a}$$

$$A_0(z) = \frac{Q}{\sqrt{2Boz + Q^2}}. \tag{2.8b}$$

By plugging these expressions into the viscous and curvature terms of (2.2b), one observes that they are both decreasing with z. Viscous and curvature terms are therefore negligible along the entire jet, if they are already negligible in the vicinity of the nozzle exit. This is satisfied if the flow rate is sufficiently large, and more precisely if the following conditions are met:

$$Q \gg 1, \tag{2.9a}$$

$$Q^2 \gg Bo, \tag{2.9b}$$

$$Q^3 \gg BoOh. \tag{2.9c}$$

It should be noted that if the parameters Q, Bo and Oh are defined from the local values of U_0 and A_0, conditions (2.9a)–(2.9c) are always satisfied sufficiently far away from the nozzle (e.g. Sauter & Buggisch 2005). Since the phenomena we will describe result from a dynamics that integrates over distances much larger than the jet initial radius, we use here (2.8b) as a good approximation of the base flow everywhere.

For simplicity, we assume in the following that Q is the only large parameter, Bo and Oh being of order 1 or smaller. Both U_0 and A_0 then vary with respect to the slow variable

$$Z = \frac{z}{z_o} + 1 \tag{2.10}$$

as

$$U_0(Z) = Q\sqrt{Z}, \tag{2.11a}$$

$$A_0(Z) = 1/\sqrt{Z}, \tag{2.11b}$$

where

$$z_o = \frac{Q^2}{2Bo} \tag{2.12}$$

is the (large) non-dimensionalized variation scale of the base flow.

2.2. *Perturbations*

We now consider linear perturbations (u_p, A_p) in velocity and cross-section to the above base flow. These perturbations satisfy the linear system

$$\frac{\partial A_p}{\partial t} = -\frac{\partial (A_p U_0 + A_0 u_p)}{\partial z}, \tag{2.13a}$$

$$\frac{\partial u_p}{\partial t} + \frac{\partial u_p U_0}{\partial z} = 3\frac{Oh}{A_0}\left\{\frac{\partial}{\partial z}\left(A_0\frac{\partial u_p}{\partial z} + A_p\frac{\partial U_0}{\partial z}\right) - \frac{A_p}{A_0}\frac{\partial}{\partial z}\left(A_0\frac{\partial U_0}{\partial z}\right)\right\} + \frac{\partial \mathcal{L}(A_p)}{\partial z}, \tag{2.13b}$$

where $\mathcal{L}(A_p)$ is the linear operator obtained by linearizing $K - K_0$ around A_0.

We want to analyse these perturbations in the 'jetting' régime when the jet is globally stable. More precisely, we do not consider the global transition that leads to dripping and which has been studied elsewhere (Le Dizès 1997; Sauter & Buggisch 2005; Rubio-Rubio *et al.* 2013). We are interested in the growth of the perturbations that give rise to the formation of droplets far away from the nozzle. In this régime, the jet is convectively unstable: the perturbations are advected downstream as they grow. We expect droplets to form when the perturbation has reached a sufficiently large amplitude. Of particular interest is the maximum amplitude that perturbations can reach at a given location z_f from a fixed level of noise. This amounts to calculating the maximum spatial gain that perturbations can exhibit at a given downstream location. For this purpose, we will consider two situations.

(i) Fluctuations are mainly present at the nozzle, as in laboratory experiments where the jet nozzle is vibrated, for instance (Sauter & Buggisch 2005). In this case, we are interested in the spatial gain at z_f of perturbations generated at the nozzle, $z = 0$.

(ii) The jet is subject to a background noise which acts at every z location. In this case, we are interested in the maximum gain at z_f of perturbations that originate from anywhere along the jet. In other words, we are interested in the spatial gain between z_i and z_f, where z_i is chosen such that the gain is maximum. Obviously, the gain in this case is larger than in (i), since $z = 0$ is one particular excitation location among the many possible in this case.

The base flow is stationary; a temporal excitation at a given location with a fixed frequency leads to a temporal response in the whole jet with the same frequency. As the jet can be forced on A or on u, we expect two independent spatial structures associated with each frequency. If we write

$$(u_p, A_p) = (\tilde{u}, \tilde{A})e^{-i\omega t} + \text{c.c.,} \qquad (2.14)$$

the normalized solution forced in u at the nozzle will satisfy $\tilde{A}(z = 0) = 0$, $\tilde{u}(z = 0) = 1$, while the one forced in A at the nozzle will satisfy $\tilde{A}(z = 0) = 1$, $\tilde{u}(z = 0) = 0$. A linear combination of these two solutions can be used to obtain the normalized solution forced in u or forced in A at any location z_i.

We then define a spatial gain in A from z_i to z_f from the solution forced in A at z_i by $G_A(z_i, z_f) = |\tilde{A}(z_f)|$. Similarly, we define a spatial gain in u from z_i to z_f from the solution forced in u at z_i by $G_u(z_i, z_f) = |\tilde{u}(z_f)|$.

Both U_0 and A_0 depend on the slow spatial variable Z. Anticipating that the typical wavelength will be of order 1, a local plane wave approximation (WKBJ approximation) can be used (Bender & Orszag 1978). In other words, each time-harmonic perturbation amplitude can be written as a sum of expressions of the form (WKBJ approximation)

$$(\tilde{u}, \tilde{A}) = (v(Z), a(Z))e^{iz_o \int^Z k(s)\,ds}, \qquad (2.15)$$

where $k(Z)$, $v(Z)$ and $a(Z)$ depend on the slow variation scale of the base flow. With the WKBJ ansatz, the perturbation equations become at leading order in $1/z_o$

$$(-i\omega + ikU_0)a + ikA_0v = 0, \qquad (2.16a)$$

$$(-i\omega + ikU_0)v = -3Ohk^2v + \frac{ik}{2A_0^{3/2}}(1 - k^2A_0)a. \qquad (2.16b)$$

These two equations can be simultaneously satisfied (by non-vanishing fields) if and only if

$$(-\mathrm{i}\omega + \mathrm{i}kU_0)^2 + 3Ohk^2(-\mathrm{i}\omega + \mathrm{i}kU_0) - \frac{k^2}{2\sqrt{A_0}}(1 - k^2 A_0) = 0. \qquad (2.17)$$

This equation provides k as a function of Z. Expressions for $v(Z)$ and $a(Z)$ can be obtained by considering the problem to the next order (see appendix B).

Among the four possible solutions to (2.17), only the two wavenumbers corresponding to waves propagating downstream are allowed. As explained in Bers (1983) (see also Huerre & Monkewitz 1990), these wavenumbers are the analytic continuations for real ω of functions satisfying $\mathrm{Im}(k) > 0$ for large $\mathrm{Im}(\omega)$. They are well defined in the convective régime that we consider here.

If $\omega = \overline{\omega}Q$ with $\overline{\omega} = O(1)$, the wavenumbers associated with the downstream propagating waves can be expanded as

$$k \sim k_0 + \frac{k_1}{Q}, \qquad (2.18)$$

where k_0 is found to be identical for both waves:

$$k_0 = \frac{\omega}{U_0} = \overline{\omega}A_0. \qquad (2.19)$$

At the order $1/Q$, we get

$$k_1 = -\mathrm{i}\left\{ \frac{k_0 A_0^{3/4}}{\sqrt{2}}\sqrt{1 - A_0 k_0^2 + \frac{9Oh^2\sqrt{A_0}k_0^2}{2}} - \frac{3Ohk_0^2 A_0}{2} \right\}. \qquad (2.20)$$

The two wavenumbers are obtained by considering the two possible values of the square root. Although both waves are needed to satisfy the boundary conditions at the nozzle, the solution is rapidly dominated downstream by a single wave corresponding to the wavenumber with the smallest imaginary part.

Both the solution forced in A and the solution forced in u are thus expected to have a similar WKBJ approximation (2.15). The main contribution to the two gains $G_A(z_i, z_f)$ and $G_u(z_i, z_f)$ is therefore expected to be the same and to be given by the exponential factor

$$G(z_i, z_f) = \mathrm{e}^{S(Z_i, Z_f)}, \qquad (2.21)$$

where

$$S(Z_i, Z_f) = -z_o \int_{Z_i}^{Z_f} \mathrm{Im}(k)(Z)\,\mathrm{d}Z = -\frac{z_o}{Q}\int_{Z_i}^{Z_f} \mathrm{Im}(k_1)(Z)\,\mathrm{d}Z. \qquad (2.22)$$

This implicitly assumes that $z_o/Q = Q/2Bo$ is large. When $z_o/Q = O(1)$, the WKBJ approach remains valid but the gain (2.21) is of the same order of magnitude as the variation of v and a. In this case, one should *a priori* take into account the amplitudes v and a provided in appendix B and apply the boundary conditions explicitly at the forcing location. This leads to different gains for a forcing in velocity and a forcing in radius.

The gain G is associated with the temporal growth of the local perturbation. Indeed, S can be written as

$$S = z_o \int_{Z_i}^{Z_f} \frac{\sigma(k_l(Z), Oh_l(Z))}{\tau_{c_l}(Z) U_0(Z)} \, \mathrm{d}Z, \qquad (2.23)$$

where $\sigma(k, Oh)$ is the growth rate of the capillary instability for the 1D model:

$$\sigma(k, Oh) = \frac{k}{\sqrt{2}} \sqrt{1 - k^2 + \frac{9 Oh^2 k^2}{2}} - \frac{3 Oh k^2}{2}. \qquad (2.24)$$

The local wavenumber $k_l(Z)$, local Ohnesorge number $Oh_l(Z)$ and local capillary time scale $\tau_{c_l}(Z)$ vary as

$$k_l(Z) = \overline{\omega} Z^{-3/8}, \qquad (2.25a)$$
$$Oh_l(Z) = Oh Z^{1/8}, \qquad (2.25b)$$
$$\tau_{c_l}(Z) = Z^{-3/8}. \qquad (2.25c)$$

In the following, we write S as

$$S = \frac{z_o}{\sqrt{2} Q} \overline{S}(Z_f, Z_i, Oh, \overline{\omega}), \qquad (2.26)$$

with

$$\overline{S}(Z_i, Z_f, \overline{\omega}, Oh) = \overline{\omega} \int_{Z_i}^{Z_f} z^{-7/8} \left(\sqrt{1 - \overline{\omega}^2 z^{-3/2} + \frac{9 Oh^2 \overline{\omega}^2}{2} z^{-5/4}} - \frac{3 Oh \overline{\omega}}{\sqrt{2}} z^{-5/8} \right) \mathrm{d}z. \qquad (2.27)$$

Our objective is to find the frequency $\overline{\omega}$ that gives the largest value of $\overline{S}$ at a given Z_f. For the type of perturbations in case (i) (nozzle excitation), $Z_i = 1$, and we are looking for

$$\overline{S}_{max}^{(a)}(Z_f, Oh) = \max_{\overline{\omega}} \overline{S}(1, Z_f, \overline{\omega}, Oh). \qquad (2.28)$$

For the type of perturbations in case (ii) (background noise), the gain is maximized over all Z_i between 1 and Z_f, so

$$\overline{S}_{max}^{(b)}(Z_f, Oh) = \max_{\overline{\omega}} \max_{1 \leqslant Z_i < Z_f} \overline{S}(Z_i, Z_f, \overline{\omega}, Oh). \qquad (2.29)$$

For $z > 1$, the integrand in the expression of $\overline{S}$ is always positive when $\overline{\omega} < 1$. This means that as long as $\overline{\omega}_{max}^{(a)} \leqslant 1$, the gain cannot be increased by changing Z_i, and we have $\overline{S}_{max}^{(b)} = \overline{S}_{max}^{(a)}$. When $\overline{\omega}_{max}^{(a)} > 1$, the perturbation starts to decrease before increasing further downstream. In this case, the gain can be increased by considering larger Z_i. More precisely, Z_i has to be chosen such that the integrand starts to be positive, which gives $Z_i = \overline{\omega}^{4/3}$. In this régime,

$$\overline{S}_{max}^{(b)}(Z_f, Oh) = \max_{\overline{\omega}} \overline{S}(\overline{\omega}^{4/3}, Z_f, \overline{\omega}, Oh). \qquad (2.30)$$

Both $\overline{S}_{max}^{(a)}$ and $\overline{S}_{max}^{(b)}$ are obtained using standard Matlab subroutines.
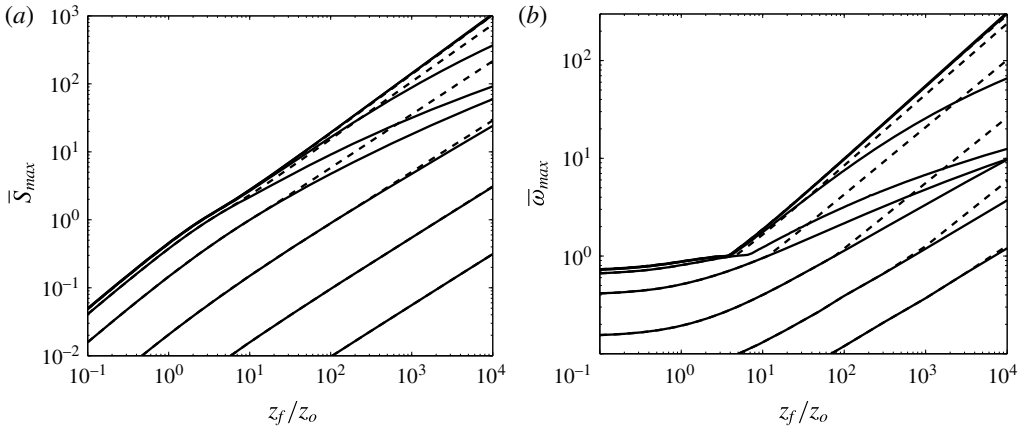
FIGURE 2. Maximum gain $\overline{S}_{max}$ (a) and most dangerous frequency $\overline{\omega}_{max}$ (b) of the perturbations excited from background noise (dashed lines) and at the nozzle (solid lines) as a function of the distance $z_f/z_o = Z_f - 1$ from the nozzle. From bottom to top, Oh takes the values 1000, 100, 10, 1, 0.1, 0.01 and 10^{-4}.

3. Quantitative results

The results of the optimization procedure are shown in figure 2 for both nozzle excitation and background noise. Both the maximum gain and the most dangerous frequency are plotted versus the rescaled distance z_f/z_o from the nozzle for Oh ranging from 10^{-4} to 10^3. The same results are shown as level curves in the $(z_f/z_o, Oh)$ plane in figure 3. As expected, $\overline{S}_{max}$ grows as z_f/z_o increases or Oh decreases (see figure 2a). The most dangerous frequency follows the same trend (see figure 2b). As already mentioned above, nozzle excitation (case (i)) and background noise (case (ii)) provide the same results when $\overline{\omega}_{max} \leqslant 1$. The contour $\overline{\omega}_{max} = 1$ has been reported in figure 3(a) as a dotted line. On the left of this dotted line, the contours of maximum gain are then the same for both cases. When $\overline{\omega}_{max}$ is larger than 1, background noise gain becomes larger than nozzle excitation gain. The most dangerous frequency for background noise also becomes larger than that for nozzle excitation. It should be noted, however, that significant differences are only observed in an intermediate régime of Oh (typically $10^{-2} < Oh < 1$) for large values of $\overline{S}$ ($\overline{S} > 5$) (see figure 3).

Figure 3 can be used to obtain the distance of the expected transition to jet breakup and droplet formation. We assume that a gain of order $G_t \approx e^7$, that is $S_t = 7$, is enough for the transition, a value commonly admitted in boundary layer instabilities (Schlichting 1987). From (2.26), we can deduce the value of $\overline{S}$ needed for transition,

$$\overline{S}_t = S_t \sqrt{2} Q/z_o = S_t 2\sqrt{2} Bo/Q \qquad (3.1)$$
$$\approx 20 Bo/Q \qquad (3.2)$$
$$= 20 \tau_c g/u_0 \qquad (3.3)$$

and from figure 3(a) the position z_f/z_o where such a value of $\overline{S}$ is reached in case (i) or (ii).

If the fluid collapses into a single drop between two pinch-offs, the distance between two droplets is given by the wavelength at breakup, $\lambda_{max} = 2\pi/A_0(z_f)/\overline{\omega}_{max}$,
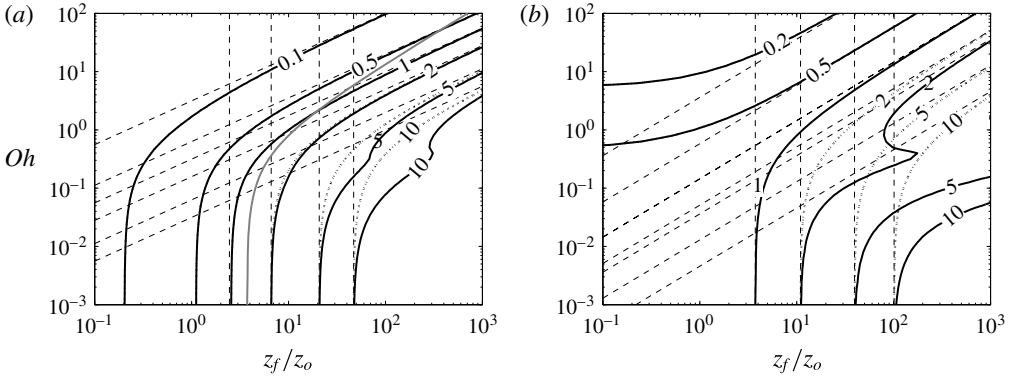
FIGURE 3. Level curves of the maximum gain $\overline{S}_{max}$ (a) and the most dangerous frequency $\overline{\omega}_{max}$ (b) of the perturbations excited from background noise (dashed lines) and at the nozzle (solid lines) in the $(z_f/z_o, Oh)$ plane. The dashed lines correspond to the asymptotic limits (3.11) and (3.5) for small and large Oh respectively. On the left of the $\omega_{max} = 1$ curve (indicated as a grey line in (a)), the solid and dashed lines are superimposed.

deduced from (2.19), and the droplet diameter is

$$d_{max} \sim [6\lambda_{max}A_0(z_f)]^{1/3} \sim \left(\frac{12\pi}{\overline{\omega}_{max}}\right)^{1/3}. \tag{3.4}$$

These two quantities are plotted in figure 4 for a few values of $\overline{S}_t$ as a function of Oh. What is particularly remarkable is that the drop diameter remains mostly constant in the full interval $10^{-3} < Oh < 10^2$ whatever the noise level for both cases (figure 4b). Yet, in this interval of Oh, the breakup distance z_f varies by a factor of 1000 (figure 3a), while the wavelength varies by a factor of 20 or more (figure 4a). In the case of background noise, z_f and λ_{max} increase with Oh. We observe the same evolution in the case of noise excitation for small $\overline{S}_t$. However, the curves of both cases depart from each other for large values of $\overline{S}_t$ (for instance $\overline{S}_t = 10$) with a surprising local peak for case (i) close to $Oh \approx 0.3$. As we shall see in §4, this peak is associated with a larger damping of the perturbation outside the instability range for moderate Oh.

In figures 3 and 4, we have also plotted the asymptotic behaviours of the different quantities obtained for large Oh and small Oh. The details of the derivation are provided in appendix A. We provide below the final result only.

3.1. *Large viscosity (large Oh)*

In the viscous régime ($Oh \gg 1$), the position z_f of breakup strongly increases with Oh, and converges to the asymptotic curve (deduced from (A 10) and (A 12))

$$z_f/z_o \sim \left(\frac{9}{2\sqrt{2}}\right)^{4/3} \overline{S}_t^{4/3} Oh^{4/3} \tag{3.5}$$

for both cases (i) and (ii) if $1 \ll z_f/z_o \ll Oh^4$. The variation in terms of Bo and Q can be obtained using (3.1) and (2.12).
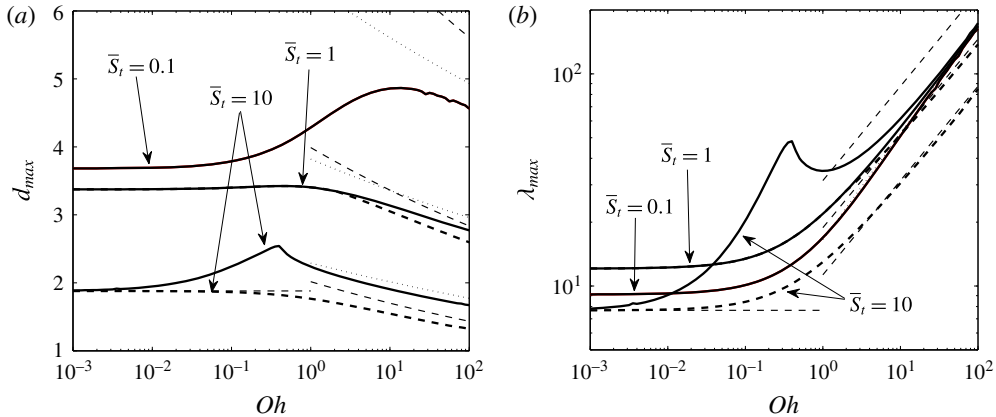
FIGURE 4. Wavelength at breakup (*a*) and resulting droplet diameter (*b*) versus *Oh* for background noise (dashed lines) and nozzle excitation (solid lines). The different curves correspond to the transition level $\bar{S}_t = 0.1$, 1, 10. The thin dashed lines correspond to the asymptotic expressions for small and large *Oh*.

This scaling law, which was also derived by Javadi *et al.* (2013), expresses that breakup occurs when the local capillary instability growth rate overcomes the stretching rate of the jet. Indeed, and coming back to dimensional quantities, the velocity and local radius vary far from the nozzle as $U_0 \sim \sqrt{2gz}$ and $h \sim \sqrt{Q^*}/(2gz)^{1/4}$ respectively, where $Q^* = U_0 h^2$ is the dimensional flow rate. The local stretching rate is then given by $\partial_z U_0 \sim \sqrt{g/(2z)}$ while the viscous capillary growth rate based on the current radius is of order $\gamma/(\eta h) = \gamma(2gz)^{1/4}/(\eta\sqrt{Q^*})$. The latter overcomes the former at a distance z_f of order $(\eta/\gamma)^{4/3} g^{1/3}(Q^*)^{2/3}$. In terms of dimensionless parameters, this gives

$$z_f/h_0 \propto Oh^{4/3} Bo^{1/3} Q^{2/3}, \tag{3.6}$$

which is essentially the scaling deduced from (3.5) if one remembers that $\bar{S}_t \propto Bo/Q$ and $z_o \propto Q^2/Bo$.

In this viscous régime, the most dangerous frequencies are not the same in cases (i) and (ii). This implies that the wavelength λ_{max} at the point of transition and the droplet diameter d_{max} are also different. For case (i), we obtain from (A 9) and (3.5)

$$\overline{\omega}_{max}^{(a)} \sim \alpha_a \bar{S}_t^{2/3} Oh^{1/6}, \quad \text{with } \alpha_a = \frac{3^{3/4}}{2^{7/4}} \approx 0.678, \tag{3.7}$$

which gives

$$\lambda_{max}^{(a)} \sim \beta_a Oh^{1/2}, \quad \text{with } \beta_a = 4\pi 3^{1/4} \approx 16.54, \tag{3.8a}$$

$$d_{max}^{(a)} \sim \gamma_a \bar{S}_t^{-2/9} Oh^{-1/18}, \quad \text{with } \gamma_a = \pi^{1/3} 3^{1/12} 2^{15/12} \approx 3.82. \tag{3.8b}$$

For case (ii), we obtain from (A 11) and (3.5)

$$\overline{\omega}_{max}^{(b)} \sim \alpha_b \bar{S}_t^{8/9} Oh^{2/9}, \quad \text{with } \alpha_b = \frac{3}{2^{7/3}} \approx 0.595, \tag{3.9}$$

which gives

$$\lambda_{max}^{(b)} \sim \beta_b \bar{S}_t^{-2/9} Oh^{4/9}, \quad \text{with } \beta_b = 2^{31/12}\pi \approx 18.83, \tag{3.10a}$$

$$d_{max}^{(b)} \sim \gamma_b \overline{S}_t^{-8/27} Oh^{-2/27}, \quad \text{with } \gamma_b = \pi^{1/3} 2^{13/9} \approx 3.99. \quad (3.10b)$$

A naive local argument like the one leading to equation (3.6) would predict for λ_{max} the most unstable local wavelength at z_f. As will be shown in §5, this fails in making the correct predictions, precisely because it ignores the stretching history of the fluid particles and of the corresponding unstable modes. Equation (3.6) is thus consistent with a local argument, but the local argument does not incorporate the whole truth.

3.2. *Low viscosity (small Oh)*

In the weakly viscous régime ($Oh \ll 1$), both noise and nozzle excitations are expected to give the same breakup distance z_f. This distance is well approximated by

$$z_f/z_o \approx \eta_0 \overline{S}_t^{8/7}, \quad \text{with } \eta_0 \approx 3.45, \quad (3.11)$$

when $z_f/z_o > 3.74$, that is $\overline{S}_t > 1.32$.

Again, as in the previous viscous limit, this scaling law expresses that breakup occurs when the local capillary instability growth rate overcomes the stretching rate. The local jet stretching rate is still $\partial_z U_0 \sim \sqrt{g/(2z)}$ while the inviscid capillary growth rate based on the current radius is now of order $\sqrt{\gamma/\rho h^3} = \sqrt{\gamma/\rho}(2gz)^{3/8}/(Q^*)^{3/4}$. The latter overcomes the former at a distance of order $(Q^*)^{6/7} g^{1/7} (\rho/\gamma)^{4/7}$. In terms of dimensionless parameters, this gives

$$z_f/h_0 \propto Bo^{1/7} Q^{6/7}, \quad (3.12)$$

which is essentially the scaling in (3.11) with $\overline{S}_t \propto Bo/Q$ and $z_o \propto Q^2/Bo$.

In this régime, the most dangerous frequency is also the same in both cases and is given by

$$\overline{\omega}_{max} = \alpha_0 \overline{S}_t^{6/7}, \quad \text{with } \alpha_0 \approx 0.79, \quad (3.13)$$

which gives

$$\lambda_{max} \sim \beta_0 \overline{S}_t^{-2/7}, \quad \text{with } \beta_0 \approx 14.82, \quad (3.14a)$$

$$d_{max} \sim \gamma_0 \overline{S}_t^{-2/7}, \quad \text{with } \gamma_0 \approx 3.63. \quad (3.14b)$$

Again, and for the same reason, naive local scaling fails in representing these scaling laws adequately.

4. Comparison with three-dimensional predictions

In this section, we focus on the régime of intermediate values of Oh for which the asymptotic expressions do not apply. We address the peculiar behaviour of the optimal perturbation in the case of nozzle excitation in this régime. In figure 4(*a,b*), we have seen that for $\overline{S}_t = 10$ both λ_{max} and d_{max} exhibit a surprising kink around $Oh \approx 0.3$. The same non-monotonic behaviour has also been observed in the breakup distance z_f/z_0 as a function of Oh (see figure 3*a*). These surprising behaviours are associated with the particular properties of the perturbations outside the instability domain. Indeed, for large $\overline{S}_t$, the optimal perturbation is obtained for $\overline{\omega}_{max} > 1$. The local wavenumber of the perturbation, which is $\overline{\omega}$ at the nozzle, is then larger than 1 close to the nozzle, that is in the stable régime (see figure 5*a*). The optimal perturbation excited from
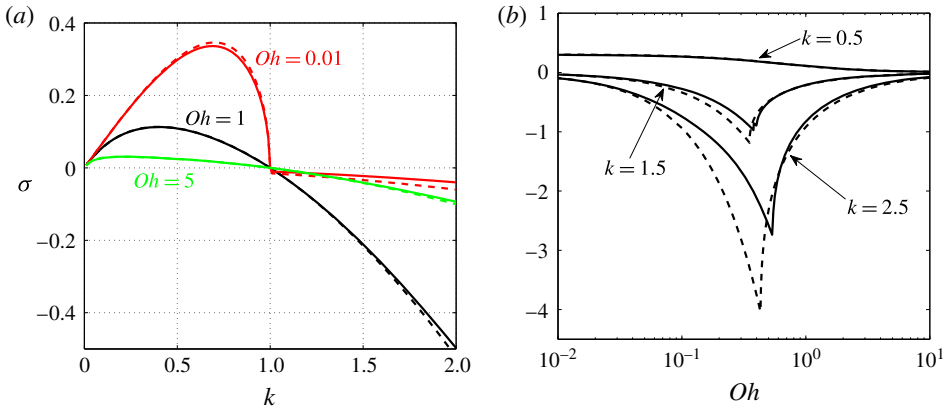
FIGURE 5. (Colour online) Comparison of 1D and 3D local dispersion relations. Solid line: 1D dispersion relation. Dashed line: 3D dispersion relation for axisymmetric modes. (*a*) Temporal growth rate versus the wavenumber k for various Oh. (*b*) Temporal growth rate versus Oh for fixed wavelengths.

the nozzle is thus first spatially damped before becoming spatially amplified. This damping régime explains the smaller gain obtained by nozzle excitation compared with background noise. It turns out that the strength of this damping is not monotonic with respect to Oh and exhibits a peak for an intermediate value of Oh. Such a peak is illustrated in figure 5, where we have plotted the (local) temporal growth rate of the perturbation versus Oh for a few values of the (local) wavenumber. We do observe that for the values of k satisfying $k \geqslant 1$, that is outside the instability band, the local growth rate exhibits a negative minimum for Oh between 0.1 and 1.

The presence of this damping régime naturally questions the validity of our one-dimensional (1D) model. The 1D model is indeed known to correctly describe the instability characteristics of three-dimensional (3D) axisymmetric modes (Eggers & Villermaux 2008). However, no such results exist in stable régimes. In fact, the 1D dispersion relation departs from the 3D dispersion relation of axisymmetric modes when $k > 1$. This departure is visible in figure 5, where we have also plotted the local growth rate obtained from the 3D dispersion relation given in Chandrasekhar (1961, p. 541). Significant differences are observed, but the 3D growth rates exhibit a similar qualitative behaviour as a function of Oh. In particular, there is still a damping rate extremum in the interval $0.1 < Oh < 1$. We can therefore expect a similar qualitative behaviour of the perturbation outside the instability range with the 3D model.

In figure 6, we compare the optimization results for the nozzle excitation obtained with the 1D model with those obtained using the 3D dispersion relation of Chandrasekhar. This is done by replacing the function $\overline{S}$ in (2.27) by

$$\overline{S}^{(3D)}(Z_i, Z_f, \overline{\omega}, Oh) = \sqrt{2} Oh \int_{Z_i}^{Z_f} (y^2(x, J) - x^2) \, \mathrm{d}z, \qquad (4.1)$$

where

$$x = x(z, \overline{\omega}) = \frac{\overline{\omega}}{z^{3/4}}, \quad J = J(z, Oh) = \frac{1}{Oh^2 z^{1/4}}, \qquad (4.2a,b)$$
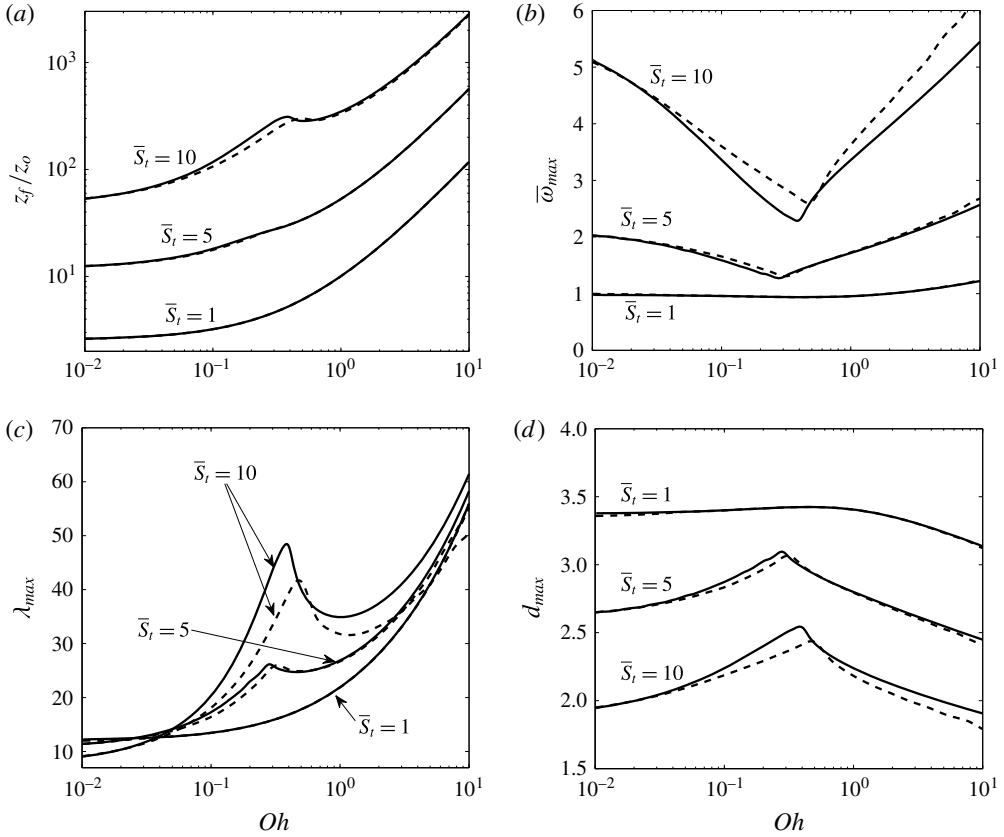
FIGURE 6. Characteristics of the response to nozzle excitation versus Oh for various values of $\bar{S}_t$ and two different stability models (solid line, 1D; dashed line, 3D axisymmetric). (*a*) Breakup distance. (*b*) Most dangerous frequency. (*c*) Wavelength at breakup. (*d*) Drop diameter.

and $y = y(x, J)$ is given by

$$2x^2(x^2 + y^2)\frac{I_1'(x)}{I_0(x)}\left[1 - \frac{2xy}{x^2 + y^2}\frac{I_1(x)I_1'(y)}{I_1(y)I_1'(x)}\right] - (x^4 - y^4) = J\frac{xI_1(x)}{I_0(x)}(1 - x^2). \qquad (4.3)$$

As expected, differences can be observed between the 1D and 3D results for the largest value of $\bar{S}_t$ ($\bar{S}_t = 10$). However, the trends remain the same. Close to $Oh \approx 0.3$, the breakup distance exhibits a plateau, the frequency a minimum, the wavelength and the drop diameter a peak. These peaks have a smaller amplitude for the 3D dispersion relation and are slightly shifted to higher values of Oh. For $\bar{S}_t = 1$, no difference between the two models is observed. This can be understood by the fact that the perturbation does not exhibit a period of damping for such a small value of $\bar{S}_t$. The 1D model therefore perfectly describes the gain of 3D perturbations, which turns out to be the same as for background noise for $Oh < 2$ (see figure 3*a*).

5. Comparison with local predictions

In this section, our goal is to compare the results of the optimization procedure with predictions obtained from the local dispersion relation. We have seen in §2 that
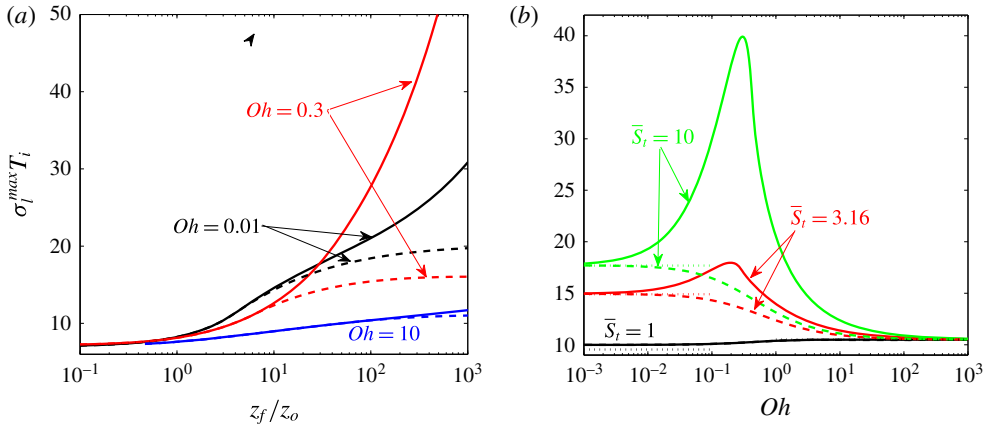
FIGURE 7. (Colour online) Maximum local temporal growth rate σ_l^{max} normalized by the free fall time T_i at the breakup location assuming breakup for a gain e^7 (solid line, nozzle excitation; dashed line, background noise). (*a*) Variation with respect to the breakup location z_f/z_o for different Oh. (*b*) Variation with respect to Oh for different values of $\bar{S}_t$. The dotted lines in (*b*) are the asymptotic predictions (5.5*a*) and (5.5*b*).

the gain can be related to the local temporal growth rate of the perturbation along the jet (see expression (2.23)). Both the local capillary time scale τ_{c_l} and the Ohnesorge number Oh_l vary with Z (see expressions (2.25*b*), (2.25*c*)). At a location Z, the maximum temporal growth rate (normalized by the capillarity time at the nozzle) is given by

$$\sigma_l^{max}(Z) = \frac{Z^{3/8}}{2\sqrt{2} + 6OhZ^{1/8}}, \quad (5.1)$$

and is reached for the wavelength (normalized by h_0) (see Eggers & Villermaux 2008)

$$\lambda_l(Z) = \frac{2\pi}{Z^{1/4}}\sqrt{2 + 3\sqrt{2}OhZ^{1/8}}. \quad (5.2)$$

If we form a drop from this perturbation wavelength at this location, we would then obtain a drop diameter (normalized by h_0)

$$d_l(Z) = \frac{(12\pi)^{1/3}}{Z^{1/4}}\left(2 + 3\sqrt{2}OhZ^{1/8}\right)^{1/6}. \quad (5.3)$$

As the local growth rate increases downstream, a simple upper bound of the gain is then obtained by taking the exponential of the product of the maximum growth rate by the time T_i needed to reach the chosen location. The time T_i is the free fall time given by

$$T_i = \frac{Q}{Bo}(\sqrt{Z} - 1). \quad (5.4)$$

In figure 7, we have plotted the product $\sigma_l^{max}T_i$ at the location predicted for the transition assuming that a gain e^7 is needed for such a transition. In figure 7(*a*), this quantity is plotted as a function of the transition location z_f/z_o. As expected, we obtain the chosen value for the transition (i.e. 7) for small z_f/z_o. For large z_f/z_o, the product $\sigma_l^{max}T_i$ also goes to a constant for background noise whatever the
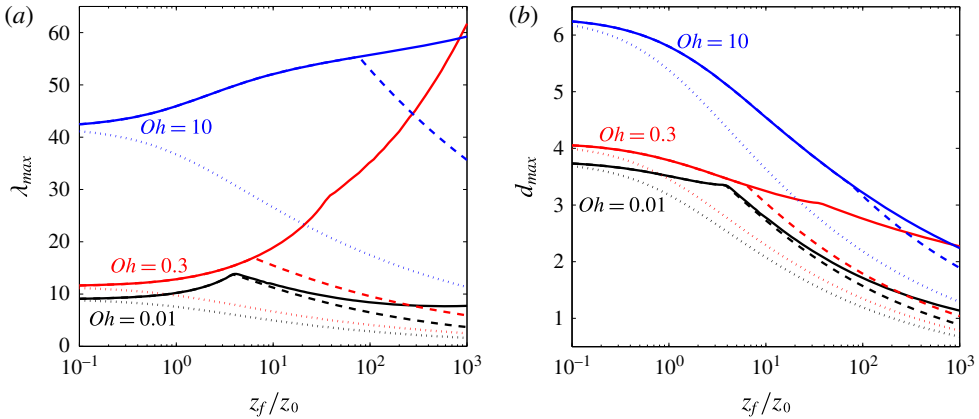
FIGURE 8. (Colour online) Wavelength at breakup (*a*) and drop diameter (*b*) versus the breakup location z_f/z_o for various values of *Oh* (solid line, nozzle excitation; dashed line, background noise).

Ohnesorge number. However, it has a contrasted behaviour for nozzle excitation, with an important increase with z_f/z_o for the value $Oh = 0.3$.

In figure 7(*b*), $\sigma_l^{max} T_i$ is plotted as a function of *Oh*, for different values of $\overline{S}_t$, that is for different values of the ratio Bo/Q in view of (3.1). For large and small *Oh*, we recover the estimates deduced using (3.5) and (3.11),

$$\sigma_l^{max} T_i \sim 10.5 \quad \text{as } Oh \to \infty, \tag{5.5a}$$

$$\sigma_l^{max} T_i \sim 20.68 - 11.14 \overline{S}_t^{-4/7} \quad \text{as } Oh \to 0. \tag{5.5b}$$

For background noise, $\sigma_l^{max} T_i$ varies smoothly between these two extreme values. A completely different evolution is observed for nozzle excitation: a local peak forms between $0.1 < Oh < 1$ with an amplitude increasing with $\overline{S}_t$. This phenomenon is related to the damping of the optimal perturbation discussed in the previous section. We have indeed seen that for nozzle excitation, large gain (that is large $\overline{S}_t$) is obtained for perturbations exhibiting a damping period prior to their growth. Thus, the growth has to compensate a loss of amplitude. As the damping is strongest for intermediate *Oh*, the transition is pushed the farthest for these values, explaining the largest growth of the $Oh = 0.3$ curve in figure 7(*a*) and the peaks of figure 7(*b*).

We have seen that the optimal procedure provides a wavelength and a droplet size as a function of *Z* and *Oh* only. These quantities are compared with the local estimates (5.2) and (5.3) in figure 8. Both nozzle excitation (solid lines) and background noise (dashed lines) are considered for $Oh = 0.01$, 0.3 and 10. We observe that the local predictions (dotted lines) always underestimate the wavelength and the drop diameter. For the wavelength, the ratio with the local estimate typically increases with z_f/z_o and *Oh*. The gap is the strongest for the nozzle excitation case, especially for intermediate *Oh* (see the curve for $Oh = 0.3$), for which the local estimate is found to underestimate the wavelength by a factor as high as 25 for $z_f/z_o = 10^3$.

In contrast to the wavelength, the drop diameter follows the same trend as the local prediction as a function of z_f/z_o. For both noise excitation and background noise, the diameter decreases with the breakup location.

For large or small Oh, the behaviours of the wavelength and drop diameter obtained by the optimization procedure and local consideration can be directly compared using the results obtained in appendix A. For large Oh, the local prediction reads

$$\lambda_l/h_0 \sim \beta_l Oh^{1/2} Z_f^{-3/16}, \quad \text{with } \beta_l = 2\pi 2^{1/4}\sqrt{3} \approx 12.94, \tag{5.6a}$$

$$d_l/h_0 \sim \gamma_l Oh^{1/6} Z_f^{-11/49}, \quad \text{with } \gamma_l = (2\pi)^{1/3}(3\sqrt{2})^{1/6} \approx 2.35, \tag{5.6b}$$

while the optimization procedure gives

$$\lambda_{max}^{(a)}/h_0 \sim \beta^{(a)} Oh^{1/2}, \quad \text{with } \beta^{(a)} \approx 16.54, \tag{5.7a}$$

$$\lambda_{max}^{(b)}/h_0 \sim \beta^{(b)} Oh^{2/3} Z_f^{-1/6}, \quad \text{with } \beta^{(b)} \approx 22.83, \tag{5.7b}$$

$$d_{max}^{(a)}/h_0 \sim \gamma^{(a)} Oh^{1/6} Z_f^{-1/6}, \quad \text{with } \gamma^{(a)} \approx 4.63, \tag{5.7c}$$

$$d_{max}^{(b)}/h_0 \sim \gamma^{(b)} Oh^{2/9} Z_f^{-2/9}, \quad \text{with } \gamma^{(b)} \approx 5.16. \tag{5.7d}$$

For small Oh, the local estimates are

$$\lambda_l^{nv}/h_0 \sim \beta_l^{nv} Z_f^{-1/4}, \quad \text{with } \beta_l^{nv} \approx 2\pi\sqrt{2} \approx 8.88, \tag{5.8a}$$

$$d_l^{nv}/h_0 \sim \gamma_l^{nv} Z_f^{-1/4}, \quad \text{with } \gamma_l^{nv} = (12\pi)^{1/3}(2)^{1/6} \approx 3.76, \tag{5.8b}$$

while the optimization procedure gives for $Z_f > 4.74$ (see appendix A)

$$\lambda_{max}/h_0 \sim \beta^{nv} Z_f^{-1/4}, \quad \text{with } \beta^{nv} \approx 20.20, \tag{5.9a}$$

$$d_{max}/h_0 \sim \gamma^{nv} Z_f^{-1/4}, \quad \text{with } \gamma^{nv} \approx 4.94. \tag{5.9b}$$

6. Applications

We now apply the results to a realistic configuration obtained from a nozzle of radius $h_0 = 1$ mm in a gravity field with $g = 9.81$ m s^{-2}. We consider three fluids: water (at 20°), for which $\gamma \approx 72 \times 10^{-3}$ N m^{-1}, $\nu \approx 10^{-6}$ m^2 s^{-1}, and two silicone oils of surface tension $\gamma \approx 21 \times 10^{-3}$ N m^{-1} and of viscosity $\nu \approx 5 \times 10^{-5}$ m^2 s^{-1} and $\nu \approx 3 \times 10^{-4}$ m^2 s^{-1}. For these three fluids, we take $\rho \approx 10^3$ kg m^{-3} as a fair order of magnitude.

For water, we obtain $Oh = 3.7 \times 10^{-3}$, $Bo = 0.13$ and a parameter $Q = 3.72 u_0$, with the velocity u_0 at the nozzle expressed in m s^{-1}. For the silicone oils, we get $Bo = 0.46$ and $Q = 6.9 u_0$ and two values of Oh: $Oh = 0.46$ and $Oh = 2$. The conditions of validity (2.9a)–(2.9c) of the inertial solution then require u_0 to be (much) larger than $u_c = 0.26$ m s^{-1} for the water and $u_c = 0.15$ m s^{-1} for the silicone oils.

In figure 9, we have plotted the theoretical predictions for the breakup location, the frequency, the wavelength and the drop diameter as the fluid velocity at the nozzle is varied from u_c to $10 u_c$, that is for Q varying from 1 to 10. We have chosen $S_t = 7$ for the background noise transition and $S_t = 4$ for the transition by the nozzle excitation. A smaller value of S_t has been chosen for the nozzle excitation to describe controlled conditions of forcing. Figure 9(a) shows that for the three fluids the transition by the nozzle excitation can be reached before the background noise transition. The values obtained for the breaking length are comparable to the experimental values reported in Javadi *et al.* (2013). They measured a normalized breaking length of order 100–150 for silicone oil of $\nu \approx 5 \times 10^{-5}$ m^2 s^{-1} from a nozzle of the same diameter for flow rates ranging from $Q = 0.5$ to $Q = 1.3$.
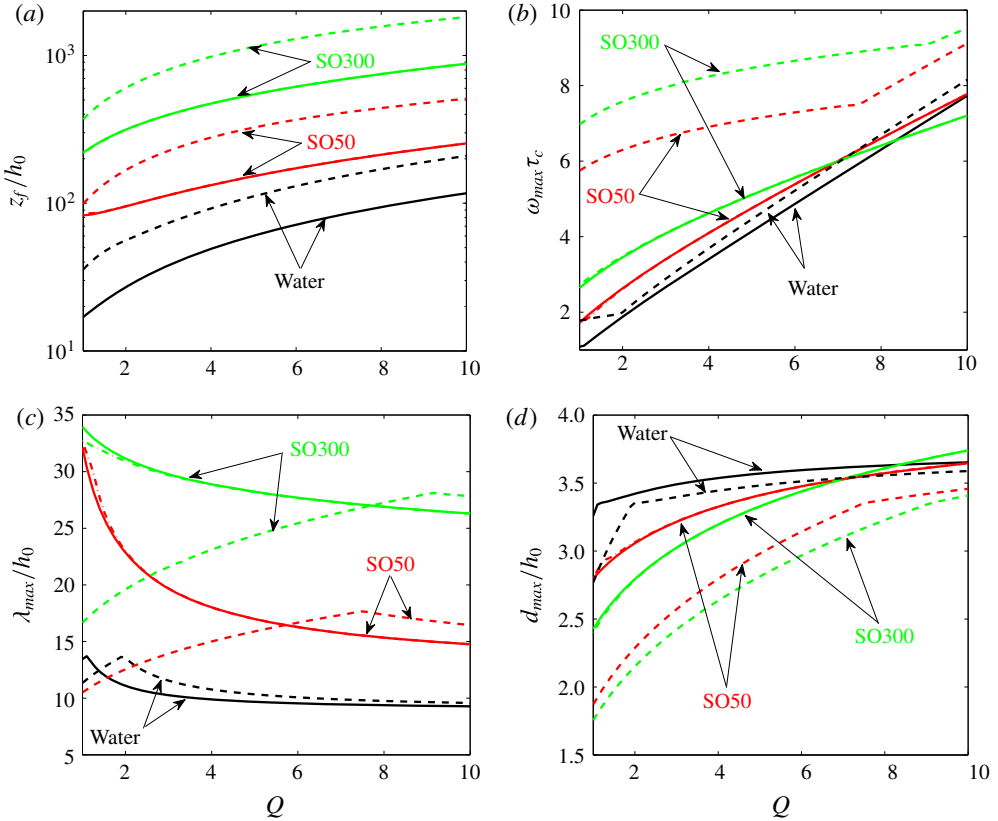
FIGURE 9. (Colour online) Characteristics at breakup by nozzle excitation or background noise for a jet of radius $h_0 = 1$ mm assuming that breakup occurs when the perturbation gain has reached e^{S_t} (solid lines, nozzle excitation with $S_t = 4$; dot–dash lines, nozzle excitation with $S_t = 4$ using the 3D dispersion relation; dashed lines, background noise with $S_t = 7$; black lines, water; red lines, silicone oil of $\nu = 5 \times 10^{-5}$ m^2 s^{-1} (SO50); green lines, silicone oil of $\nu = 3 \times 10^{-4}$ m^2 s^{-1} (SO300)). (*a*) Breakup location; (*b*) most dangerous frequency; (*c*) wavelength at breakup; (*d*) drop diameter.

Figure 9(*b*) provides the most dangerous frequency of the excitation. For the three cases, the frequency for the nozzle excitation is relatively close to the neutral frequency Q of the jet at the nozzle. For both silicone oils, this frequency is, however, much smaller than the frequency obtained by the background noise transition, especially for small Q.

The breakup wavelength shown in figure 9(*c*) exhibits a different behaviour with respect to the flow rate Q for the nozzle excitation and the background noise. It decreases monotonically with Q for the noise excitation while it increases for the background noise up to an extremum before starting to decrease. For the three fluids, noise excitation provides a larger wavelength than background noise for small Q, but the opposite is observed above a critical value of Q which increases with Oh. It should be noted that for small Q, the wavelengths obtained for noise excitation are comparable for both silicone oils. Both curves would even cross if a larger value of S_t was considered. This property is related to the non-monotonic behaviour of the breakup wavelength already discussed above (see figure 6*c*).

In contrast to the wavelength, the droplet size (figure 9*d*) does not change much with Q and is comparable for the three fluids. Nozzle excitation provides larger droplets, but this effect is significant for the smallest values of Q only.

Finally, it should be noted that the differences between the 1D and 3D predictions for the nozzle excitation are barely visible. A very small departure of the wavelength curves can be seen for the silicone oils only. This confirms both the usefulness and the validity of the 1D model.

7. Conclusion and final remarks

At the end of this detailed study, we are now in a position to answer the questions raised in the introduction. The breakup distance from the orifice of a jet falling by its own weight can indeed be understood by comparing two time scales. The relevant time scales are the capillary destabilization time (viscous, or not) based on the local jet radius, and the inverse of the local jet stretching rate. Breakup occurs, in both viscous and inviscid régimes, as discussed in § 3, when the latter overcomes the former, a fact that was already known (Villermaux 2012; Javadi *et al.* 2013). However, we have also learned that this aspect is only a tiny piece of the problem as a whole. This simple local rule, if naively extended to estimation of the wavelength of the perturbation breaking the jet, would predict that the wavelength is proportional to the local jet radius in the inviscid case, for instance. This prediction was found to always underestimate the wavelength at breakup. The most dangerous wavelength and the drop diameter account for the stretching history of the fluid particles as they travel along the jet; this is the reason why their values are different depending on whether the perturbations are introduced at the jet nozzle only or through a background noise affecting the jet all along its extension. An optimal theory computing the gain of every mode as the jet deforms and accelerates was thus necessary to answer the – seemingly simple – question of its breakup. It has, in addition, revealed the existence of an unexpected non-monotonic dependence of the most dangerous wavelength λ_{max} with respect to *Oh*.

We have also provided quantitative results assuming that a spatial gain of e^7 of the linear perturbations is sufficient for breakup. This value of the critical gain is an *ad hoc* criterion which assumes a particular level of noise and which neglects the possible influence of the nonlinear effects. It would be interesting to test this criterion with experimental data.

Our analysis has focused on a capillary jet whose base state is in an inertial régime. Close to the nozzle, especially if the flow rate is small, a viscous dominated régime is expected (Senchenko & Bohr 2005). We have not considered such a régime here. However, a similar WKBJ analysis could *a priori* be performed with a base flow obtained by resolving the more general equations (2.2) if the jet variation scale remains large compared with the perturbation wavelength. However, far from the nozzle, the jet always becomes inertial. The growth of the perturbation is therefore expected to be the same as described above. For this reason, the optimal perturbation obtained from background noise could be the same. Indeed, we have seen that in order to reach a large gain ($\bar{S}_t > 5$ or so), the optimal perturbation should be introduced far from the nozzle. If the jet is in the inertial régime at this location, the same gain is then obtained. This point was already noticed in Javadi *et al.* (2013).

For nozzle excitation, the entire evolution of the jet contributes to the optimal perturbation. We have seen that large gains ($\bar{S}_t > 5$) are obtained by perturbations that exhibit a spatial damping before starting to grow. We have also seen that

this damping régime is only qualitatively described by the 1D model. We do not expect a better description if the jet is dominated by viscous effects. Moreover, it is known that in this régime non-parallel effects are also important close to the nozzle (Rubio-Rubio *et al.* 2013), which invalidates the WKBJ approach. For this régime, it would be interesting to perform an optimal stability analysis using more advanced tools (Schmid 2007) to take into account non-parallel effects and non-modal growth.

It should be noted finally that we have computed the perturbation gain by considering the exponential terms of the WKBJ approximation only. A better estimate could readily be obtained by considering the complete expression of the WKBJ approximation. This expression, which has been provided in appendix B, involves an amplitude factor that contains all of the other contributions affecting the growth of the perturbation. Different expressions are obtained for A and u, which, in particular, implies that different gains are obtained for the velocity and the jet radius. It is important to mention that the other contributions are not limited to a simple correcting factor associated with the local stretching (Tomotika 1936; Eggers & Villermaux 2008). Other contributions associated with the z-dependence of the local wavenumber and local jet profile are equally important, leading to expressions that are not simple even in the large- or small-Oh limit.

Acknowledgement

Appendix A. Asymptotic régimes

In this appendix, we provide asymptotic expressions for $\overline{S}_{max}$ and $\overline{\omega}_{max}$ in the viscous and inviscid régimes, that is for $Oh \to \infty$ and $Oh \to 0$ respectively.

A.1. *Maximum gain in the viscous régime* ($Oh \to \infty$)

When $Oh \to \infty$, the expression of the integrand in (2.27) can be simplified, and in the whole domain of integration, we can use the approximation

$$\sqrt{1 - \overline{\omega}^2 z^{-3/2} + \frac{9Oh^2 \overline{\omega}^2}{2} z^{-5/4}} \sim \sqrt{1 + \frac{9Oh^2 \overline{\omega}^2}{2} z^{-5/4}} - \frac{\overline{\omega}^2 z^{-3/2}}{2\sqrt{1 + \frac{9Oh^2 \overline{\omega}^2}{2} z^{-5/4}}}, \quad \text{(A 1)}$$

such that (2.27) can be written as

$$\overline{S} \sim \frac{\overline{S}_1(Z_i, Z_f, X_\omega)}{Oh} - \frac{\overline{S}_2(Z_i, Z_f, X_\omega)}{Oh^3}, \quad \text{(A 2)}$$

with

$$\overline{S}_1(Z_i, Z_f, X_\omega) = X_\omega^{-3/4} \int_{Z_i X_\omega}^{Z_f X_\omega} X^{-7/8} \left(\sqrt{1 + \frac{9}{2X^{5/4}}} - \frac{3}{\sqrt{2} X^{5/8}} \right) \mathrm{d}X, \quad \text{(A 3a)}$$

$$\overline{S}_2(Z_i, Z_f, X_\omega) = X_\omega^{-1/2} \int_{Z_i X_\omega}^{Z_f X_\omega} \frac{X^{-19/8}}{2\sqrt{1 + \frac{9}{2X^{5/4}}}} \, \mathrm{d}X \quad \text{(A 3b)}$$

and

$$X_\omega = (Oh\overline{\omega})^{-8/5}. \quad (A\,4)$$

When Z_f is not too large, we are in the following configuration.
(1) $Z_i X_\omega \ll 1$ and $Z_f X_\omega \ll 1$. In this case, we can write

$$\overline{S}_1 \sim \frac{2\sqrt{2}}{9}(Z_f^{3/4} - Z_i^{3/4}) - \frac{X_\omega^{5/4}}{108\sqrt{2}}(Z_f^2 - Z_i^2) + O(X_\omega^{5/2} Z_f^{13/4}), \quad (A\,5a)$$

$$\overline{S}_2 \sim \frac{2\sqrt{2}}{9 X_\omega^{5/4}}\left(\frac{1}{Z_i^{3/4}} - \frac{1}{Z_f^{3/4}}\right) + O(Z_f^{1/2}), \quad (A\,5b)$$

which gives

$$\overline{S} \sim \frac{2\sqrt{2}}{9 Oh}(Z_f^{3/4} - 1 - \overline{\omega}^2 + \overline{\omega}^2 Z_f^{-3/4}) - \frac{Z_f^2 - 1}{108\sqrt{2} Oh^3 \overline{\omega}^2} + O\left(\frac{Z_f^{1/2}}{Oh^3}, \frac{Z_f^{13/4}}{Oh^5 \overline{\omega}^4}\right) \quad (A\,6)$$

in case (i) (nozzle excitation) and

$$\overline{S} \sim \frac{2\sqrt{2}}{9 Oh}(Z_f^{3/4} - 2\overline{\omega} + \overline{\omega}^2 Z_f^{-3/4}) - \frac{Z_f^2 - \overline{\omega}^{8/3}}{108\sqrt{2} Oh^3 \overline{\omega}^2} + O\left(\frac{Z_f^{1/2}}{Oh^3}, \frac{Z_f^{13/4}}{Oh^5 \overline{\omega}^4}\right) \quad (A\,7)$$

in case (ii) (background noise) with $Z_i = \overline{\omega}^{4/3}$.

In case (i), the maximum gain is obtained for

$$\overline{\omega}_{max}^{(a)} \sim \left(\frac{Z_f^2 - 1}{48 Oh^2 (1 - Z_f^{-3/4})}\right)^{1/4}, \quad (A\,8)$$

that is

$$\overline{\omega}_{max}^{(a)} \sim \frac{Z_f^{1/2}}{2\,3^{1/4} Oh^{1/2}} \quad (A\,9)$$

for large Z_f, and equals

$$\overline{S}_{max}^{(a)} \sim \frac{2\sqrt{2} Z_f^{3/4}}{9 Oh}\left(1 - Z_f^{-3/4} - \frac{Z_f^{1/4}}{2\sqrt{3} Oh}\right) + O\left(\frac{Z_f^{1/4}}{Oh^2}, \frac{Z_f^{5/4}}{Oh^3}\right). \quad (A\,10)$$

In case (ii), the maximum gain is obtained for

$$\overline{\omega}_{max}^{(b)} \sim \frac{Z_f^{2/3}}{48^{1/3} Oh^{2/3}} \quad (A\,11)$$

and equals

$$\overline{S}_{max}^{(b)} \sim \frac{2\sqrt{2} Z_f^{3/4}}{9 Oh}\left(1 - \frac{3^{2/3}}{2^{4/3} Oh^{2/3} Z_f^{1/12}}\right). \quad (A\,12)$$

The condition that $Z_f X_\omega^{max} \ll 1$ does not give any restriction in case (ii). However, it requires in case (i)

$$Z_f \ll Oh^4. \quad (A\,13)$$
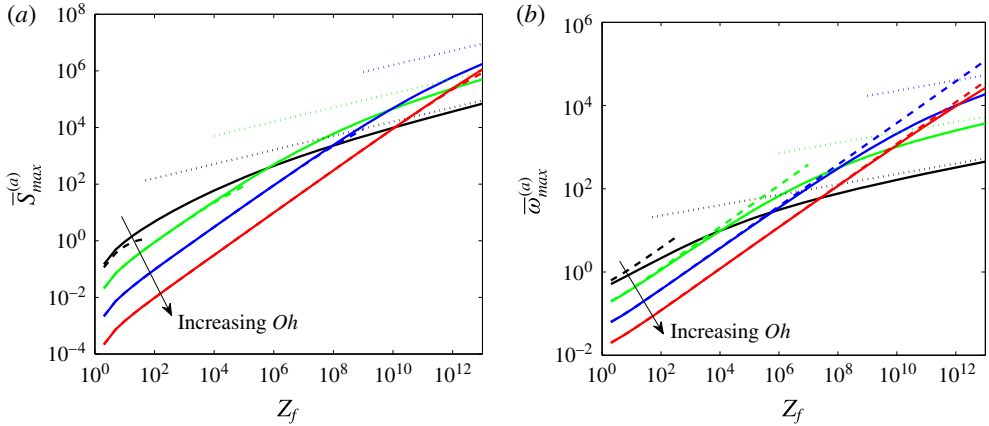
FIGURE 10. (Colour online) Maximum gain $\overline{S}_{max}^{(a)}$ (a) and most dangerous frequency $\overline{\omega}_{max}^{(a)}$ (b) of the perturbations excited at the nozzle as a function of the distance Z_f from the nozzle (solid lines, numerical results; dashed and dotted lines, asymptotic results obtained for large Oh for $Z_f \ll Oh^4$ (formulae (A 10) and (A 9)) and $Z_f \gg Oh^4$ (formulae (A 17) and (A 16)) respectively). Here, Oh takes the values 1, 10, 100 and 1000.

When $Z_f \gg Oh^4$, another limit has to be considered for case (i).

(2) $Z_i X_\omega \ll 1$ and $Z_f X_\omega \gg 1$. In this limit, we have

$$\overline{S}_1 \sim \frac{8Z_f^8}{X_\omega^{5/8}} - \frac{I_o}{X_\omega^{3/4}}, \qquad (A\,14a)$$

$$\overline{S}_2 \sim \frac{2\sqrt{2}}{9X_\omega^{5/4}Z_i^{3/4}}. \qquad (A\,14b)$$

It gives

$$\overline{S} \sim 8Z_f^{1/8}\overline{\omega} - I_o\overline{\omega}^{6/5}Oh^{1/5} - \frac{2\sqrt{2}\overline{\omega}^2}{9Oh} + O\left(\frac{Z_f^{1/2}}{Oh^3}, \frac{Z_f^{13/4}}{Oh^5\overline{\omega}^4}\right), \qquad (A\,15)$$

which is maximum for

$$\overline{\omega}_{max}^{(a)} \sim 9\sqrt{2}OhZ_f^{1/8}. \qquad (A\,16)$$

The maximum gain equals

$$\overline{S}_{max}^{(a)} \sim 36\sqrt{2}Z_f^{1/4}Oh. \qquad (A\,17)$$

This estimate applies only when $Z_f \gg Oh^4$.

The asymptotic formulae are compared with numerical results in figure 10 for case (i) and figure 11 for case (ii). In both cases, we have plotted the maximum gain $\overline{S}_{max}$ and the most dangerous frequency (the frequency that provides the maximum gain) versus Z_f for $Oh = 1$, 10, 100 and 1000. It is interesting to see that in case (i) the maximum gain and the most dangerous frequency both collapse onto a single curve when plotted as a function of the variable Z_f/Oh^4 with an adequate normalization (see figure 12).
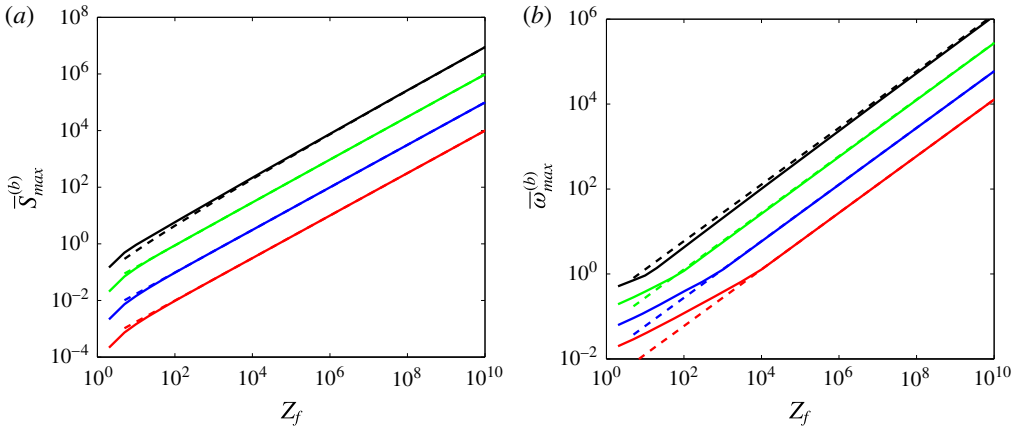
FIGURE 11. (Colour online) Maximum gain $\overline{S}_{max}^{(b)}$ (a) and most dangerous frequency $\overline{\omega}_{max}^{(b)}$ (b) of the perturbations excited from background noise as a function of the distance $\hat{Z}_f$ from the nozzle (solid lines, numerical results; dashed lines, asymptotic results (formulae (A 12) and (A 11))). From top to bottom, Oh takes the values 1, 10, 100 and 1000.
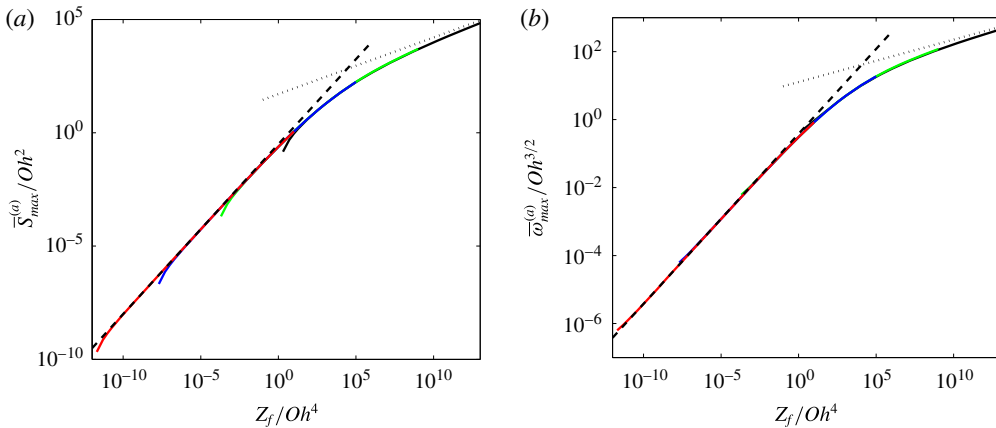
FIGURE 12. (Colour online) The same plots as figure 10 but with rescaled variables versus Z_f/Oh^4. In (a), the dotted line is (A 17) while the dashed line is the first term of (A 10). In (b), the dotted and dashed lines are (A 16) and (A 9) respectively.

A.2. *Maximum gain in the inviscid régime* $(Oh \rightarrow 0)$

When Oh is small, viscous effects come into play if we go sufficiently far away for the nozzle because the local Ohnesorge number increases algebraically with the distance to the nozzle.

Here, we shall assume that we remain inviscid in the whole domain of integration, that is

$$\sqrt{1 - \overline{\omega}^2 z^{-3/2} + \frac{9Oh^2\overline{\omega}^2}{2}z^{-5/4}} - \frac{3}{\sqrt{2}}\overline{\omega}Ohz^{-5/8} \sim \sqrt{1 - \overline{\omega}^2 z^{-3/2}}. \tag{A 18}$$
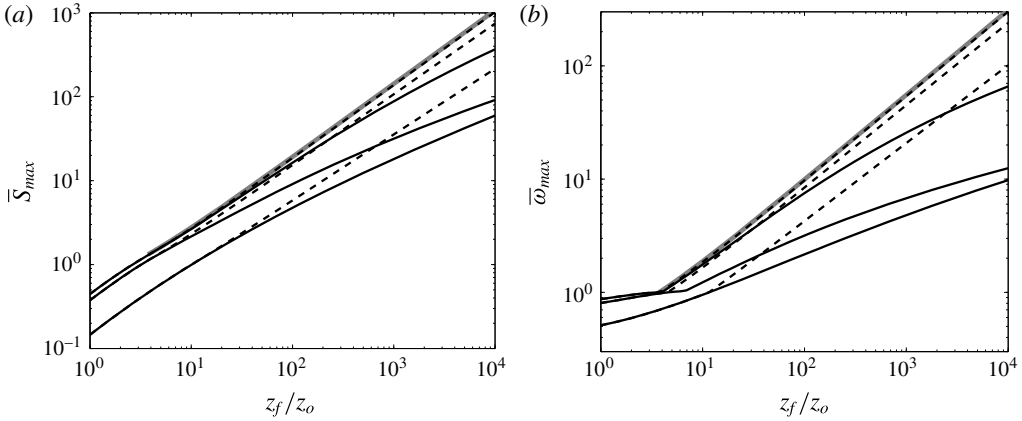
FIGURE 13. Maximum gain $\overline{S}_{max}$ (*a*) and most dangerous frequency $\overline{\omega}_{max}$ (*b*) of the perturbations excited from background noise (dashed lines) and at the nozzle (solid lines) as a function of the distance $z_f/z_o = Z_f - 1$ from the nozzle. From bottom to top, *Oh* takes the values 0.1, 0.01 and 0.001. The formulae (A 22) and (A 21) are indicated as solid grey lines in (*a*) and (*b*) respectively.

This is satisfied if $Z_f \ll Oh^{-8}$. The gain can then be written as

$$\overline{S} \sim Y_\omega^{-7/8} \int_{Z_i Y_\omega}^{Z_f Y_\omega} s^{-7/8} \sqrt{1 - s^{-3/2}} \, ds, \tag{A 19}$$

with $Y_\omega = \overline{\omega}^{-4/3}$.

Because in the inviscid limit, perturbations are neutral when they do not grow, cases (i) and (ii) provide the same gain.

For $1 < Z_f < Z_f^c \approx 4.74$, the maximum gain is reached for $\overline{\omega} < 1$, i.e. $Y_\omega > 1$. The location Z_f^c is given by the vanishing of $\partial_{Y_\omega} \overline{S}$ for $Y_\omega = 1$ and $Z_i = 1$:

$$-\frac{7}{8} \int_1^{Z_f^c} s^{-7/8} \sqrt{1 - s^{-3/2}} \, ds + (Z_f^c)^{1/8} \sqrt{1 - (Z_f^c)^{-3/2}} = 0. \tag{A 20}$$

For $Z_f^c < Z_f \ll Oh^{-8}$, the maximum gain is reached for

$$\overline{\omega}_{max} \sim \left(\frac{Z_f}{Z_f^c} \right)^{3/4} \approx 0.311 Z_f^{3/4} \tag{A 21}$$

and equals

$$\overline{S}_{max} = \beta Z_f^{7/8}, \tag{A 22}$$

where

$$\beta = (Z_f^c)^{-7/8} \int_1^{Z_f^c} s^{-7/8} \sqrt{1 - s^{-3/2}} \, ds \approx 0.338. \tag{A 23}$$

This estimate is compared with numerical values in figure 13. We do observe a convergence of the maximum gain and most dangerous frequency curves towards the inviscid limit as *Oh* decreases. It should be noted, however, that the convergence is slower for nozzle excitation (case (i)).

Appendix B. WKBJ analysis

In this section, we provide the full expression of the WKBJ approximation of each downward propagative wave. Each wave is searched for in the form

$$(u_p, A_p) = (v(Z), a(Z))e^{iz_o \int^Z k(s)\,ds}e^{-i\omega t}, \tag{B 1}$$

where $k(Z)$, $v(Z)$ and $a(Z)$ depend as the base flow on the slow spatial variable $Z = z/z_o + 1$, $z_o = Q^2/(2Bo)$ being a large parameter.

If we plug expression (B 1) into (2.13), we get up to $O(1/z_o^2)$ terms

$$(-i\omega + ikU_0)a + ikA_0v = -\frac{1}{z_o}\frac{\partial(aU_0 + vA_0)}{\partial Z}, \tag{B 2a}$$

$$(-i\omega + ikU_0)v + 3Ohk^2v - \frac{ik}{2A_0^{3/2}}(1 - k^2A_0)a$$

$$= -\frac{1}{z_o}\frac{\partial(vU_0)}{\partial Z} + \frac{3iOh}{z_o}\left(\frac{k}{A_0}\frac{\partial A_0}{\partial Z}v + 2k\frac{\partial v}{\partial Z} + \frac{\partial k}{\partial Z}v + \frac{k}{A_0}\frac{\partial U_0}{\partial Z}a\right)$$

$$- \frac{1}{4z_oA_0^{5/2}}\left(2A_0(1 + 3k^2A_0)\frac{\partial a}{\partial Z} + \frac{\partial A_0}{\partial Z}(3 - 2k^2A_0)a + 6k\frac{\partial k}{\partial Z}A_0^2a\right). \tag{B 2b}$$

These equations give at leading order (2.16*a*), (2.16*b*), from which we can deduce the dispersion relation (2.17) that defines $k(Z)$. If we now replace v on the right-hand side of (B 2*a*) by its leading-order expression in terms of a, we obtain an expression for v valid up to $O(1/z_o^2)$ terms:

$$v = \frac{1}{kA_0}\left((\omega - kU_0)a - \frac{1}{z_o}\frac{\partial(\omega a/k)}{\partial Z}\right). \tag{B 3}$$

Plugging this expression into (B 2*b*) with $U_0 = Q/A_0$, we obtain the following equation for $a(z)$:

$$R(Z)\frac{\partial a}{\partial Z} + \left(S(Z)\frac{\partial A_0}{\partial Z} + T(Z)\frac{\partial k}{\partial Z}\right)a = 0, \tag{B 4}$$

with

$$R(Z) = -2A_0k^3 + 6A_0^2k^5 + 4A_0^{3/2}k\left(\omega^2 - 3Ohik^2\omega + \frac{Qk^2(-Q + 6iOhA_0k^3)}{A_0^2}\right), \tag{B 5a}$$

$$S(Z) = \frac{-8Q\omega k^2A_0 + 3k^2(4Q^2 + A_0^{3/2} + 4iOh\omega A_0^2) - 24iOhQA_0k^4 - 2A_0^{5/2}k^5}{A_0^{3/2}}, \tag{B 5b}$$

$$T(Z) = 2A_0^{1/2}(-2\omega^2A_0 + 6iOhQk^3 + 3A_0^{3/2}k^4). \tag{B 5c}$$

This equation is valid for both downward and upward propagating waves.

For large Q, it can be simplified for the downward propagating wavenumbers using $\omega = \overline{\omega}Q$ and $k \sim \overline{\omega}A_0 + k_1/Q$ as

$$(-2k_1A_0 + 3i\overline{\omega}^2OhA_0^4)\frac{\partial a}{\partial Z} + \left(5k_1\frac{\partial A_0}{\partial Z} - A_0\frac{\partial k_1}{\partial Z}\right)a = 0, \tag{B 6}$$

where $k_1(Z)$ is given by (2.20). The amplitude $v(Z)$ is then deduced from $a(Z)$ using (B 3) at leading order in Q,

$$v(Z) = -\frac{Q}{\bar{\omega} A_0^3} k_1 a(Z). \tag{B 7}$$

The two downward propagating waves possess different expressions for k_1, and thus different amplitudes a and v. This guarantees that a combination of the two downward propagating waves can be formed such that at the orifice $a = 1$ and $v = 0$ or $a = 0$ and $v = 1$.

In the inviscid régime ($Oh \ll 1$), equation (B 6) can be integrated explicitly for any A_0 as

$$a^{(i)}(z) = C \frac{A_0^{5/2}(z)}{\sqrt{k_1(z)}}, \tag{B 8}$$

where C is a constant. It is interesting to compare this expression with the expression $a \sim A_0$ that would have been obtained by the argument of Tomotika (1936), that is by considering the solution as a uniformly stretched fluid cylinder (see Eggers & Villermaux 2008).

REFERENCES

BENDER, C. M. & ORSZAG, S. A. 1978 *Advanced Mathematical Methods for Scientists and Engineers*. McGraw-Hill.

BERS, A. 1983 *Space–Time Evolution of Plasma Instabilities – Absolute and Convective*, vol. 1, chap. 3.2. North-Holland.

CHANDRASEKHAR, S. 1961 *Hydrodynamic and Hydromagnetic Stability*. Clarendon.

CLARKE, N. S. 1969 The asymptotic effects of surface tension and viscosity on an axially-symmetric free jet of liquid under gravity. *Q. J. Mech. Appl. Maths* **22**, 247–256.

EGGERS, J. & VILLERMAUX, E. 2008 Physics of fluid jets. *Rep. Prog. Phys.* **71**, 1–79.

FRANKEL, I. & WEIHS, D. 1985 Stability of a capillary jet with linearly increasing axial velocity (with application to shaped charges). *J. Fluid Mech.* **155**, 289–307.

FRANKEL, I. & WEIHS, D. 1987 Influence of viscosity on the capillary instability of a stretching jet. *J. Fluid Mech.* **185**, 361–383.

HUERRE, P. & MONKEWITZ, P. A. 1990 Local and global instabilities in spatially developing flows. *Annu. Rev. Fluid Mech.* **22**, 473–537.

JAVADI, A., EGGERS, J., BONN, D., HABIBI, M. & RIBE, N. M. 2013 Delayed capillary breakup of falling viscous jets. *Phys. Rev. Lett.* **110** (14), 144501.

LE DIZÈS, S. 1997 Global modes in falling capillary jets. *Eur. J. Mech.* (B/*Fluids*) **16** (6), 761–778.

RUBIO-RUBIO, M., SEVILLA, A. & GORDILLO, J. M. 2013 On the thinnest steady threads obtained by gravitational stretching of capillary jets. *J. Fluid Mech.* **729**, 471–483.

SAUTER, U. S. & BUGGISCH, H. W. 2005 Stability of initially slow viscous jets driven by gravity. *J. Fluid Mech.* **533**, 237–257.

SCHLICHTING, H. 1987 *Boundary Layer Theory*. McGraw-Hill.

SCHMID, P. J. 2007 Nonmodal stability theory. *Annu. Rev. Fluid Mech.* **39**, 129–162.

SENCHENKO, S. & BOHR, T. 2005 Shape and stability of a viscous thread. *Phys. Rev.* E **71**, 056301.

TOMOTIKA, S. 1936 Breaking up of a drop of viscous liquid immersed in another viscous fluid which is extending at a uniform rate. *Proc. R. Soc. Lond.* A **153** (879), 302–318.

TROUTON, F. T. 1906 On the coefficient of viscous traction and its relation to that of viscosity. *Proc. R. Soc. Lond.* A **77**, 426–440.

VILLERMAUX, E. 2012 The formation of filamentary structures from molten silicates: Pele's hair, angel hair, and blown clinker. *C. R. Méc.* **340**, 555–564.

WEBER, C. 1931 Zum Zerfall eines Flüssigkeitsstrahles. *Z. Angew. Math. Mech.* **2**, 136–154.